Journal of the European Ceramic Society **32** (2012) p.3313

Effects of sintering temperature on the internal barrier layer capacitor (IBLC) structure in CaCu3Ti4O12 (CCTO) ceramics

Rainer Schmidt[a,*], Martin C. Stennett[b], Neil C. Hyatt[b], Jan Pokorny[b,c], Jesús Prado-Gonjal[d], Ming Li[b], Derek C. Sinclair[b]

[a] *Universidad Complutense de Madrid, Dpt. Física Aplicada III, GFMC, Facultad de Ciencias Físicas, 28040 Madrid, Spain*
[b] *The University of Sheffield, Materials Science and Engineering, Mappin Street, Sheffield S1 3JD, United Kingdom*
[c] *Academy of Sciences of the Czech Republic, Institute of Physics, Na Slovance 2, 182 21 Prague 8, Czech Republic*
[d] *Universidad Complutense de Madrid, Dpt. Química Inorgánica, Facultad de Ciencias Químicas, 28040 Madrid, Spain*

Abstract

The formation of the internal barrier layer capacitor (IBLC) structure in $CaCu_3Ti_4O_{12}$ (CCTO) ceramics was found to be facilitated by the ceramic heat treatment. Electrically insulating grain boundary (GB) and semi-conducting grain interior areas were characterized by impedance spectroscopy to monitor the evolution of the IBLC structure with increasing sintering temperature T_S (975–1100 °C). The intrinsic bulk and GB permittivity increased by factors of ≈2 and 300, respectively and the bulk resistivity decreased by a factor of $\approx 10^3$. These trends were accompanied by increased Cu segregation from the CCTO ceramics as detected by scanning electron microscopy and quantitative energy dispersive analysis of X-rays. The chemical changes due to possible Cu-loss in CCTO ceramics with increasing T_S are small and beyond the detection limits of X-ray absorption spectroscopy near Cu and Ti K-edges and Raman Spectroscopy.

Keywords: B. Grain boundaries; C. Dielectric properties; C. Chemical properties; D. Perovskites; E. Capacitors

1. Introduction

The ternary oxide compound $CaCu_3Ti_4O_{12}$ (CCTO) is a 1:3 A-site ordered perovskite ($A'A''_3B_4O_{12}$) where the oxygen octahedra are strongly tilted and the A″ site Cu cations adopt a fourfold square-planar coordination. The CCTO unit cell is a doubled simple perovskite cell and is commonly indexed as cubic Im-3. CCTO has attracted great interest due to its exceptionally high dielectric permittivity value ε'[1–9]; in CCTO ceramics the highest values reported are ≈300,000.[10,11] It is now established that the origins of such high permittivity values are extrinsic in nature[10,12] and are commonplace phenomena in a large range of CCTO based compounds.[7,13] In polycrystalline CCTO ceramics such extrinsic effects have been identified as an internal barrier layer capacitor (IBLC) structure, consisting of semi-conducting grains separated by thin insulating grain boundaries (GBs) leading to high ε' values.[12,14,15] Furthermore, a sample-electrode interface effect has been suggested to contribute to the high permittivity as well,[16] especially in single crystals where GBs are absent.[17]

A typical ceramic IBLC structure is depicted in Fig. 1a where semi-conducting (bulk) grain interiors are shown in grey whereas the surrounding insulating grain boundary areas are colorless. No percolation path for high conductivity is available and the macroscopic direct current (dc) resistance is insulating. By carrying out alternating current (ac) impedance spectroscopy (IS) it appears that at sufficiently high frequencies a sharp drop in dielectric permittivity occurs in ε' vs f plots and the giant extrinsic GB value ε_2 reduces to a bulk relative dielectric permittivity ε_1 of ≈100 (Fig. 1b).[18,19] This is the typical behavior of an IBLC structure, where the sharp permittivity drop occurs when the mean electron conduction path permitted by the applied alternating voltage signal decreases below the average grain size at increased frequency. The high frequency dielectric response is, therefore, dominated by the conducting bulk (grains) and the low frequency response by the insulating GB contribution.

---

[*] Corresponding author.
E-mail address: rainerxschmidt@googlemail.com (R. Schmidt).

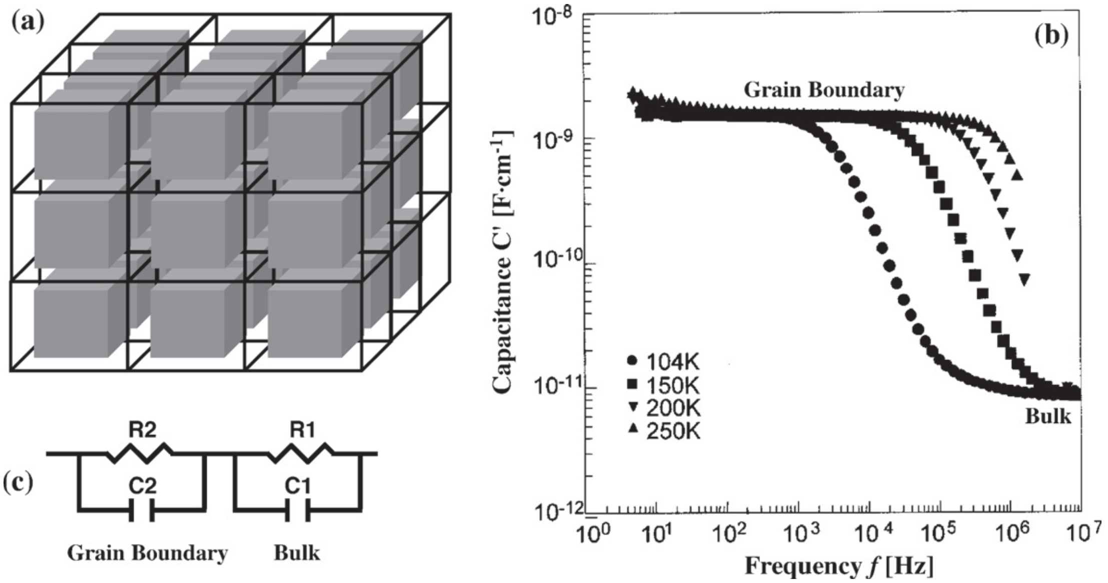

Fig. 1. Internal barrier layer capacitor (IBLC) structure in CCTO: (a) Ceramic grains are represented schematically by cubes (solid lines). The semi-conducting (grain) bulk areas are represented by smaller grey cubes. The surrounding insulating grain boundary areas are colorless. No percolation path for high conductivity is available and the macroscopic dc resistance is insulating. (b) Impedance spectroscopy (IS) data from CCTO ceramics represented in the notation of the real part of capacitance C' (effectively ε') vs frequency. Image reproduced from Ref.[4] with permission from the American Institute of Physics (AIP). (c) Idealized equivalent circuit model to account for GB and bulk dielectric relaxation processes.

Both dielectric relaxation processes (GB and bulk) can each be described ideally by one parallel resistor–capacitor circuit (RC element) and the macroscopic behavior can be represented by a series circuit of two RC elements as demonstrated in Fig. 1c. The resistors R1 and R2 correspond to the bulk and GB resistivity (ρ_1 and ρ_2), respectively and the capacitors C1 and C2 represent bulk and GB permittivity (ε_1 and ε_2), respectively. In CCTO ceramics the inhomogeneous dielectric behavior can be rather pronounced: GB and bulk resistivity can differ by a factor of up to $\approx 10^5$, and the activation energy, E_a, associated with either bulk or GB conduction processes can differ by up to a factor of $\approx$10.[20,21] Especially the large difference in E_a is a strong indicator that different charge transport mechanisms and, therefore, significant chemical differences between GB and bulk areas must exist. Despite considerable previous research efforts, such underlying chemical differences between GB and bulk in CCTO are still not yet fully understood. Especially the low bulk resistivity in nominally insulating stoichiometric $CaCu_3Ti_4O_{12}$ has lead to controversial discussions over potential non-stoichiometry to be responsible for inducing semi-conductivity. Whereas in thin films the formation of oxygen vacancies has been reported,[22] such claims had been negated in polycrystalline ceramics[23] and the most frequently postulated explanation in the literature is Cu deficiency on the A$''$ CCTO lattice site.[24,25] Direct chemical evidence though for any of the postulated solid solution models explaining non-stoichiometry has not been encountered so far. In this work the differences between GB and bulk in CCTO are elucidated by studying the effect of sintering temperature T_S on the ceramic IBLC structure in terms of the conducting bulk and insulating GB dielectric relaxations which were separately analyzed by using temperature dependent IS (10–320 K). Increasing T_S from 975 to 1100 °C leads to a factor of $\approx 10^3$ decrease in bulk resistivity ρ_1, an increase in GB permittivity ε_2 by a factor of $\approx$300 and an increase of bulk dielectric permittivity ε_1 by a factor of $\approx$2. As the dielectric properties of both the bulk and GB regions show high sensitivity to heat treatment, it seems reasonable that the large differences between such bulk and GB dielectric properties may themselves also be related to the heat treatment. It is shown here that the step-feature in the ε' vs f plot (Fig. 1b) evolves and becomes more pronounced with increasing T_S, thus supporting the hypothesis of increasing dielectric inhomogeneity as a result of the evolving chemical differences between GB and bulk with increasing T_S.

Attempts to directly measure any underlying chemical/crystallographic differences in CCTO ceramics due to variations in T_S have been made, but X-ray absorption spectroscopy near the Cu and Ti K-edges (XANES) and Raman spectroscopy failed to reveal any significant changes. Such changes must therefore be small and the dielectric properties of CCTO appear to be highly sensitive to subtle chemical and/or structural modifications. Scanning electron microscopy (SEM) operating in backscattered electron mode combined with high resolution qualitative energy dispersive analysis of X-rays (EDAX) on sintered ceramics revealed increased segregation of a Cu-rich phase with increasing T_S and accumulation on the ceramic surfaces, with the segregation being clearly visible at $T_S \approx 1050$ °C and above. For a T_S of 1100 °C, some of the Cu-rich phase appeared to volatilize as noted by an irreversible mass loss detected by thermal gravimetry. Furthermore, a subtle increase of bulk lattice parameter $\boldsymbol{a}$ with increasing T_S was detected. Quantitative EDAX spot analysis of single CCTO grains on polished ceramic surfaces provided some indication of Cu-loss from the main CCTO grain interior phase. Therefore, this work presented here supports the model of Cu deficiency in CCTO grain interior areas as a source for semi-conductivity.

2. Experimental

2.1. Powder and pellet production

$CaCu_3Ti_4O_{12}$ powder was synthesized from dried reagents of $CaCO_3$ (Aldrich, 99.995% purity), CuO (Aldrich, 99.99%) and TiO_2 (Sigma–Aldrich, 99.99%). Mixing and grinding of the precursors was performed using an agate pestle and mortar. 5 successive mixing/grinding and heat treatment cycles were required to complete the reaction and achieve good homogenization. Powder synthesis was performed at 975 °C in a Lenton muffle furnace on Pt foil for 12 and 6 h in successive cycles until the phase assemblage showed no further changes as detected by X-ray diffraction (XRD). Rapid cooling was performed by removing the Pt foils containing the CCTO powder from the furnace at temperature and quenching them on a brass block. XRD phase analysis was performed using a high-resolution STOE STADI-P diffractometer (STOE & Cie GmbH, Darmstadt) with an image plate detector, Cu K/α/1 radiation in transmission mode, operated at 40 kV and 40 mA. Six pellets were pressed from freshly crushed and ground CCTO using a uni-axial hydraulic press (1 ton) and each pellet was sintered at a different temperature, i.e. 975, 1000, 1025, 1050, 1075 and 1100 °C on Pt foil for 12 h followed by slow-cooling in the furnace. For electrical characterization by IS the pellet surfaces were first thoroughly polished and then covered on both sides with Au electrodes using dc sputtering.

2.2. Impedance spectroscopy (IS) measurements

Impedance spectra of sintered pellets were obtained in terms of separated real and imaginary parts of the complex impedance ($Z' - Z''$) over a large frequency range ($f = 10$ Hz to 2 MHz) between 10 and 320 K using an Agilent E4980A LCR meter with 100 mV amplitude of the applied ac voltage signal and an Oxford Instruments closed-cycle He refrigerator. The complex data obtained in terms of $Z' - Z''$ were converted into the permittivity $\varepsilon' - \varepsilon''$, conductivity $\sigma' - \sigma''$and modulus $M' - M''$ notations using the standard conversions.[26,27] The basic principles of IS are reviewed in the Supporting online materials, Part I.

2.3. Scanning electron microscopy (SEM) and energy dispersive analysis of X-rays (EDAX)

Scanning electron microscopy (SEM) combined with energy dispersive analysis of X-rays (EDAX) was carried out on all pellets sintered at different temperatures to investigate any changes in chemical composition and the pellet microstructure. A JEOL JSM 6400 microscope equipped with a facility for quantitative energy dispersive analysis of X-rays (EDAX) was used. The SEM was operated in backscattered electron mode with colour contrast emphasizing differences in atomic number; phases containing atoms of higher atomic number have a brighter contrast. High resolution quantitative EDAX line scans were carried out using a narrow detector opening to achieve maximum spatial resolution along the single scanning line on the pellet.

In an attempt to detect non-stoichiometry in the main CCTO phase, high resolution quantitative EDAX spot analysis on the centre of single CCTO grains with a narrow detector opening were carried out. For all sintered pellets the Ca:Cu:Ti ratios on the centre of 25 different grains were measured to obtain a statistical average for each sample. The penetration depth of the electron beam spot on one single CCTO grain was estimated to be 1–2 μm and, therefore, the main X-ray intensity detected was expected to be emitted from the CCTO grain centres irrespective of the inter-granular phase. The quantitative EDAX Ca:Cu:Ti ratios were corrected with respect to standard samples consisting of a CuTi alloy and a $CaTiO_3$ ceramic with predetermined 1:1 Cu:Ti and Ca:Ti atomic ratios. The fabrication of such standard samples is described in the Supporting online materials, Part II. Furthermore, several large area EDAX scans (≈150 μm × 150 μm) with a wide detector opening were carried out on each pellet to obtain the average surface cation concentrations.

Furthermore, the mean grain sizes for all sintered pellets were determined from the respective backscattered SEM images by averaging the size of 220 randomly selected CCTO grains on each sample and the grain size distributions were investigated.

2.4. Thermal gravimetry

Thermal gravimetry was carried out on CCTO powder synthesized at 1000 °C. A Perkin Elmer Pyris 1 thermogravimetric analyzer was used to measure the mass changes of the powder by heating up to 1100 °C. Two measurements were carried out: (A) the cooling cycle was initiated after holding the sample at 1100 °C for 60 min, and (B) the heat ramp was reversed and the cooling cycle initiated immediately after reaching 1100 °C.

2.5. Lattice parameter determination by X-ray diffraction

Small amounts of CCTO powder synthesized at 975 °C were heated at 1000, 1025, 1050, 1075 and 1100 °C on Pt foil for 12 h followed by rapid cooling on a brass block. Lattice parameter determination was achieved by mixing each powder with an internal Si standard, and the CCTO lattice parameters were determined by XRD using the STOE STADI-P diffractometer with a position sensitive detector (PSD). The CCTO lattice parameters were fitted from high angle Si and CCTO reflections using a linear least squares fitting routine provided within the WinXPOW software package.

2.6. X-ray absorption near edge spectroscopy (XANES) in CCTO for Cu and Ti K-edges

Cu K-edge and Ti K-edge X-ray absorption spectra (XAS) were acquired on beamline BL11.1 at the ELETTRA light source and on beamline X23A2 at the National Synchrotron Light Source (NSLS), respectively. In both cases, data were collected in transmission mode using CCTO powder samples, which had been heated to different temperatures followed by rapid cooling (see previous section). The powders were prepared for XAS measurements by diluting with polyethylene glycol and pressing into thin discs to afford a thickness of approximately one absorption length. Energy calibrations were achieved by using Cu and Ti metal foils measured in situ with a reference ion chamber. XAS data reduction and analysis was performed using the program ATHENA.[28]

2.7. Raman spectroscopy

Unpolarized Raman spectra were taken at room temperature on 975, 1000, 1025, 1050, 1075 and 1100 °C sintered and polished pellets using a Renishaw InVia micro-Raman spectrometer. Laser power of ≈10 mW was focused on a ≈20 μm spot. The spectrometer was equipped with a Peltier-cooled multichannel CCD detector and a diffraction grating 2400 L/mm, the slit opening was 65 μm. Spectral resolution was ≈1 cm^{-1}.

3. Results and discussion

3.1. Impedance spectroscopy

IS data were interpreted using the brick-work layer model, where bulk and GB dielectric relaxations can each be described by a parallel RC element and the macroscopic dielectric response is represented by a series connection of two RC elements (Fig. 1c).[29] IS data at 80 K for pellets sintered at different temperatures are plotted in terms of the real part of the dielectric permittivity ε' vs frequency f in Fig. 2, where two distinct permittivity plateaus are shown. In the framework of dielectric relaxations represented by RC elements, the high-permittivity plateau at low frequencies primarily originates from the GB contribution, whereas the low permittivity plateau at high frequencies (in this work termed ε_1*) primarily originates from the bulk contribution.[5] It is apparent that the low frequency GB plateau value increases substantially with increasing T_S. This increase is far too large to be explained by the changes in grain size or by the increase observed in the pellet density from ≈80 to ≈95% for T_S = 975 to 1100 °C (see Supporting online materials, Part III). From equivalent circuit analysis, it can be shown that the value of the high permittivity plateau at low frequency is a composite term involving all R and C components; however, it is entirely dominated by the C term of the GB for the data sets shown in Fig. 2. The contributions of the other components are negligible and cannot explain the strong increase in plateau magnitude with T_S. Therefore, it can be concluded that the GB permittivity in CCTO shows a substantial increase with increasing T_S. This trend was confirmed from Cole–Cole plots of ε'' vs ε' displaying one single arc, where the arc diameter represents the magnitude of the GB permittivity. Such plots are presented in the Supporting online materials, Part I. A magnification of Fig. 2a data is shown in Fig. 2b focusing on the high frequency end. It is demonstrated that the magnitude of the bulk-dominated low permittivity plateau at high frequency ε_1* increases moderately with T_S. The formal expression for the high frequency permittivity plateau ε_1* based on the RC element model (Fig. 1c) is dominated by the intrinsic bulk value ε_1 but contains a contribution from the GB permittivity ε_2. This contribution can be estimated and does not affect the general trend (see below and Supporting online materials, Part I). Therefore, the data in Fig. 2b can be interpreted as a modest increase in the bulk dielectric permittivity with T_S.

In Fig. 3 the real part of conductivity σ' is plotted vs frequency f. At low f the data are strongly frequency dependent, whereas at higher f a conductivity plateau is observed. In the framework of the brick-work layer RC element model the σ' plateau at high f represents the intrinsic bulk conductivity. From Fig. 3 it can be seen that at 80 K the bulk conductivity strongly increases by a factor of ≈100 with increasing T_S. Such increase in bulk conductivity is even stronger pronounced at lower temperatures

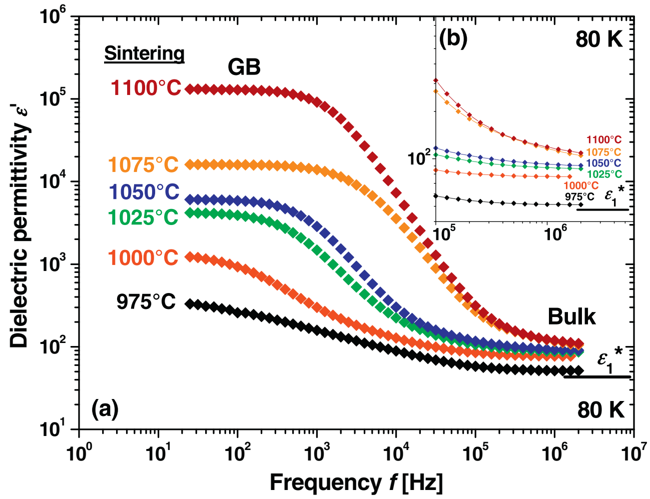

Fig. 2. (a) Real part of dielectric permittivity ε' vs frequency f [Hz] at 80 K for pellets sintered at various T_S. The magnitude of the GB plateau increases significantly with T_S. (b) High frequency behavior of ε' vs f. Axes are identical to the main figure. The bulk permittivity plateau ε_1* increases by a factor of ≈2 with increasing T_S.

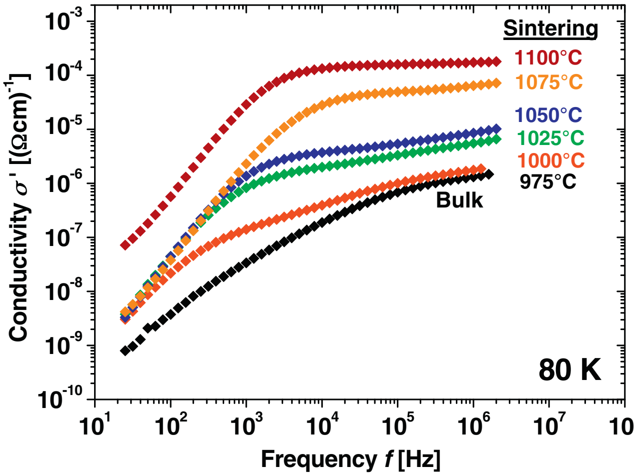

Fig. 3. Real part of conductivity σ' vs f [Hz] at 80 K for pellets sintered at various T_S. The magnitude of the high f plateau associated with the bulk dielectric relaxation increases significantly with increasing T_S indicating an increase in bulk conductivity.

as discussed below. The lower GB conductivity is expected to appear as a second low-conductivity plateau at low frequency. Indications for such a low-frequency GB relaxation can be seen in the data for $T_\mathrm{S} = 1100\,^\circ\mathrm{C}$ in Fig. 3. The GB relaxation is more clearly visible at higher temperatures, but strong overlap with a non-ohmic electrode interface relaxation was apparent, which did not allow reliable extraction of GB conductivity values and/or trends with T_S.

The reported trend of bulk conductivity σ' vs T_S was confirmed from complex plane impedance plots $-Z''$ vs Z' displaying two arcs for the bulk and GB relaxations, where the arc diameter represents the magnitude of the resistivity of the respective contribution. Such plots are presented in the Supporting online materials, Part I. For more clearly assessing the trends of all circuit parameters (Fig. 1c) with T_S quantitatively, analysis of IS data was carried out as follows:

(1) GB permittivity ε_2 was obtained from the high-permittivity plateaus at low frequency in Fig. 2 at 80 K. Contributions from the bulk dielectric relaxation were found to be negligible and therefore no correction was made to the plateau value.

(2) Bulk permittivity ε_1 was obtained from the low permittivity plateaus $\varepsilon_1{}^*$ at high frequency from data taken at 50 K, where the $\varepsilon_1{}^*$ bulk plateau is fully developed for all samples (in Fig. 2 the samples sintered at 1075 and 1100 °C do not show a full relaxation of ε' towards the bulk plateau $\varepsilon_1{}^*$ at high f). $\varepsilon_1{}^*$ values were corrected and the precise bulk permittivity ε_1 obtained by taking into account a small contribution from the GB permittivity ε_2, which was determined as described in (1).

(3) Bulk resistivity ρ_1 was calculated from the bulk permittivity ε_1 and the frequency of the bulk dielectric relaxation peaks displayed in plots of the electric modulus function M'' vs f (not shown here).

All three procedures for quantitative analysis are described in detail in the Supporting online materials, Part I. The trends of GB permittivity ε_2, bulk permittivity ε_1 and bulk resistivity ρ_1 vs T_S at selected temperatures are shown in Fig. 4. For sintering temperatures between 975 and 1100 °C the ε_2 values show a massive exponential increase with T_S by a factor of $\approx$300 (Fig. 4a). This increase is in agreement with previous work on CCTO ceramics sintered at different temperatures,[30] but is significantly more pronounced as was found in previous studies on 1100 °C sintered CCTO with different sintering time.[15,31] T_S as opposed to sintering time has a more pronounced influence on the dielectric properties of CCTO, which indicates the importance of diffusion-related phenomena occurring during the densification sintering process in CCTO ceramics.

The intrinsic bulk permittivity ε_1 shows an approximately linear increase with T_S between 1000 and 1100 °C by a factor of $\approx$2 (Fig. 4b), which can be associated with intrinsic changes of the bulk phase. Only minor parts of such increase can be associated with changes in pellet density. The rather high intrinsic ε_1 values of $\approx$100 in CCTO and related materials have been

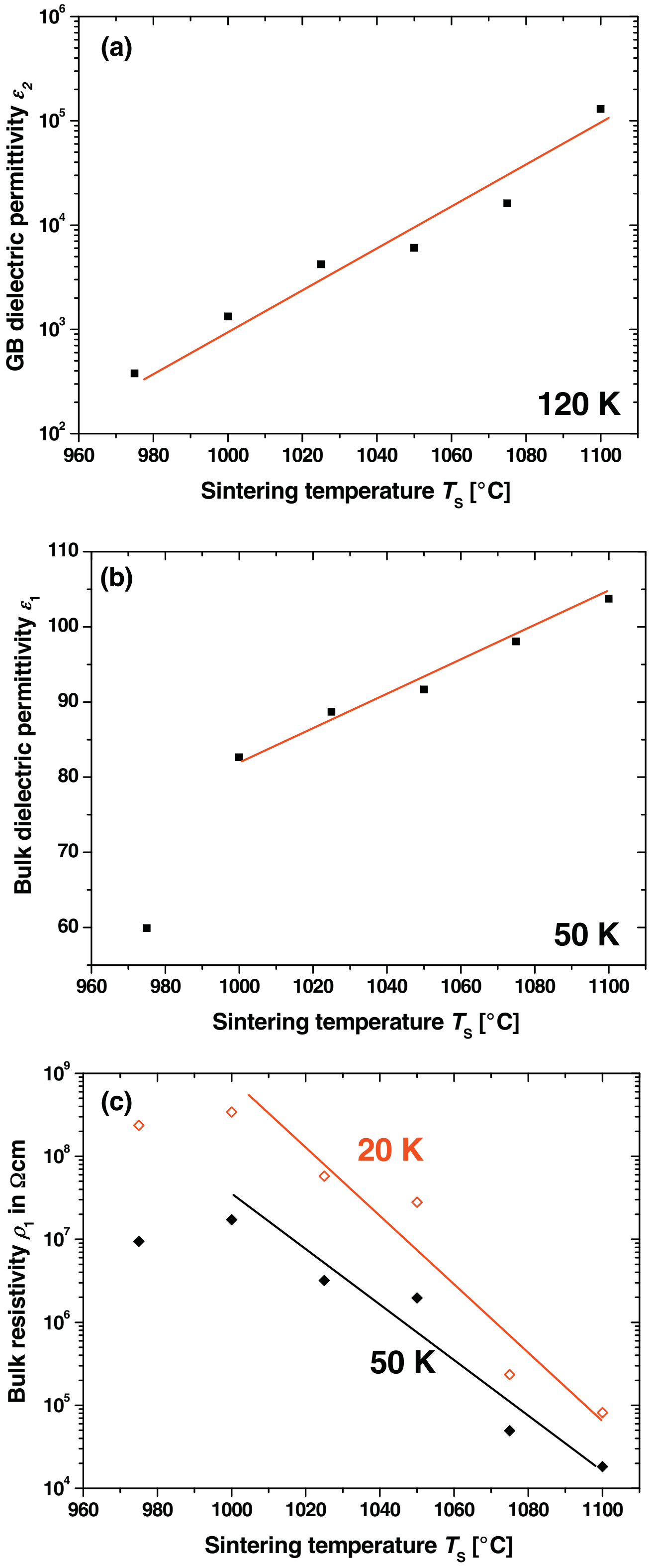

Fig. 4. (a) GB dielectric permittivity ε_2 vs T_S at 120 K. An approximately exponential increase of ε_2 with T_S is shown. (b) Bulk dielectric permittivity ε_1 vs T_S at 50 K. A linear increase of ε_1 with T_S is shown. (c) Bulk resistivity ρ_1 vs T_S at 20 (◇) and 50 K (◆). An exponential decrease of ρ_1 with T_S is shown. Solid lines are guide to the eyes.

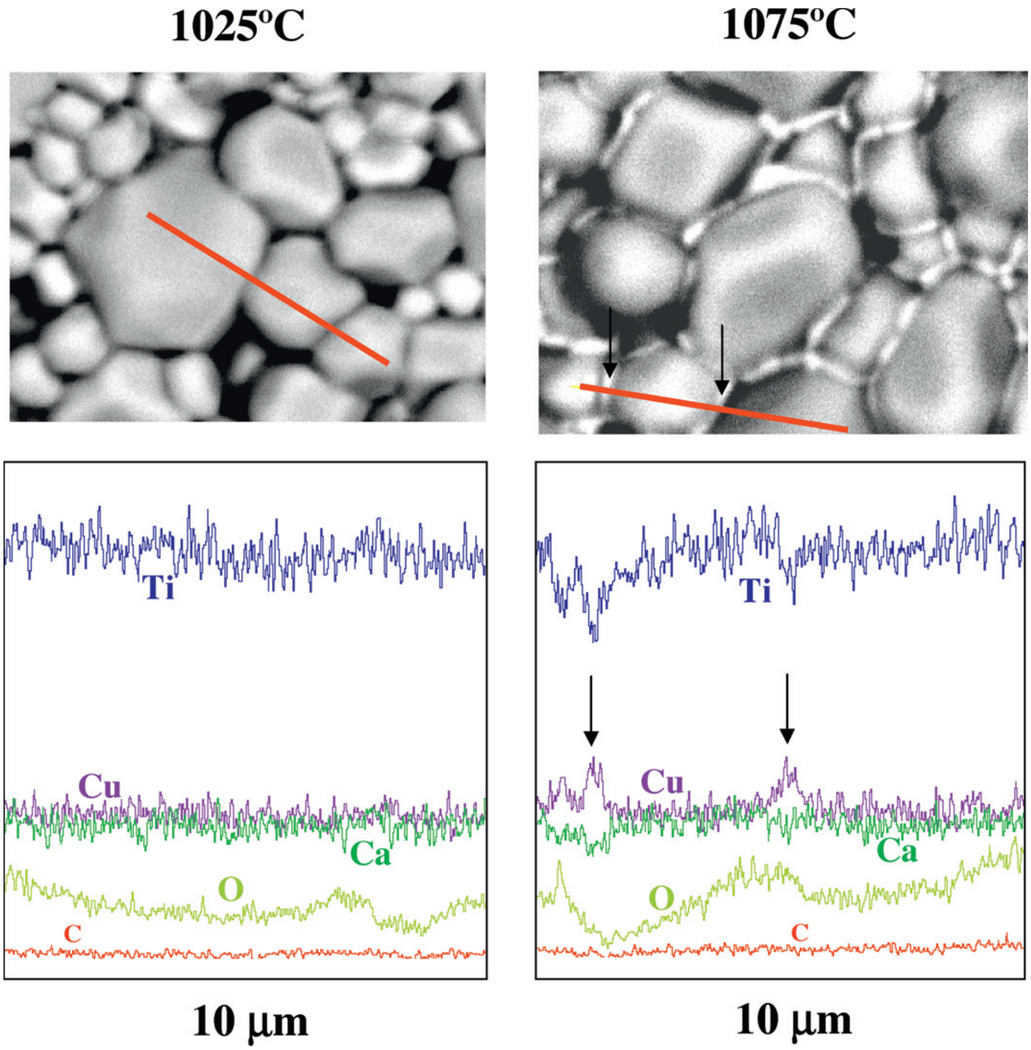

Fig. 5. SEM images collected in backscattered electron mode from unpolished surfaces of CCTO pellets sintered at 1025 and 1075 °C (first row), and EDAX line scans (second row). The solid (red) lines in the first row indicate the quantitative EDAX line scans of ≈10 µm, with the Ti, Cu, Ca and oxygen atomic concentrations along such lines being presented in the second row. Cu segregation at $T_S = 1075\,^{\circ}\mathrm{C}$ in form of an inter-granular phase is indicated. The oxygen concentration mainly reflects topographical contrast; the carbon (C) detection comes from a thin carbon layer evaporated onto the pellets to enable SEM analysis. (For interpretation of the references to color in this figure legend, the reader is referred to the web version of the article.)

associated previously with the formation of an incipient ferroelectric phase.[32] The formation of this type of phase seems to be particularly pronounced here by increasing T_S from 975 to 1000 °C.

Fig. 4c demonstrates that the bulk resistivity ρ_1 shows an exponential decrease with increasing T_S between 1000 and 1100 °C by a factor of ≈1000–4000. No such decrease can be observed though by increasing T_S from 975 to 1000 °C despite the clear increase of ε_1 mentioned above. This suggests that the increase in ε_1 may have a different source than the decrease in ρ_1. The two effects may not be directly related to each other, although both may be facilitated by the heat treatment.

The solid lines in Fig. 4 are a guide to the eyes. The changes in bulk permittivity and resistivity clearly indicate an intrinsic change in the bulk CCTO phase that is presumably related to its chemical composition. The trends of ε_1 and ε_2 vs T_S (Fig. 4a and b) are equivalent for different temperatures due to the weak temperature dependence of the bulk and GB permittivity for all samples. Contrarily, the bulk resistivity ρ_1 shows a stronger dependence on T_S at lower temperatures. Fig. 4c shows two representative data sets at 20 and 50 K where the slope of ρ_1 vs T_S increases slightly with decreasing temperature. This is consistent with Fig. 3, where the σ' vs f curves indicate a weaker dependence for 80 K.

3.2. *Scanning electron microscopy (SEM) and energy dispersive analysis of X-rays (EDAX)*

SEM images in the backscattered electron mode and EDAX line scans on the unpolished surfaces of CCTO ceramics sintered at 1025 and 1075 °C are shown in Fig. 5. EDAX data were collected from left to right along the solid (false-coloured red) lines to determine the cation concentrations. From this analysis, a Cu-rich phase starts to segregate out of the ceramics at $T_S \approx 1050\,^{\circ}\mathrm{C}$ and accumulates between the CCTO grains as an inter-granular phase (Fig. 5). This phase is clearly detectable at 1075 °C whereas there are no detectable signs of it when $T_S = 1025$ °C. EDAX point measurements for the 1075 °C sintered pellet indicated a high Cu content for the inter-granular phase (about 68%) and the remaining 32% of Ca and Ti cations may well be a proximity effect due to the adjacent CCTO phase. The segregated phase is therefore most likely copper oxide and not a Cu rich CCTO type phase. This inter-granular Cu_xO phase could not be detected by XRD, probably due to its small volume fraction. Alternatively, such Cu_xO may be amorphous and no XRD detection was therefore possible. All XRD patterns displayed evidence only for the CCTO phase to be present up to $T_S = 1100$ °C but decomposition of CCTO was indicated at $T_S = 1125$ °C.

In this case, the XRD pattern showed the presence of $CaTiO_3$, TiO_2 and small residues of the main CCTO phase, but no Cu_xO phase was detected. Furthermore, no signs of Cu_xO phase are detectable in the SEM backscattered images either after sintering at 1125 °C (see Supporting online materials, Part III). This may be understood within the following scenario: Cu_xO segregation is clearly visible above $T_S = 1050$ °C leading to a Cu-deficient CCTO grain interior phase and a range of Cu-deficient compositions $CaCu_{3-y}Ti_4O_{12}$ may exist, constituting a small solid solution ($y \geq 0$ would be small and close to zero). Cu segregation occurs towards the grain boundary areas, which may therefore contain higher Cu content than the bulk. At higher T_S such segregation may intensify and the increasing Cu-deficiency in the bulk phase may ultimately lead to the decomposition of the CCTO phase, where the segregated Cu_xO may volatilize. Cu_xO volatilization is supported by thermal gravimetry results presented below in the next section. Since increasing Cu_xO segregation and volatilization was the only clear visible change of the CCTO phase with increasing T_S, the substantial increase in conductivity of the CCTO grain interior bulk with T_S may be explained by Cu-deficiency ($CaCu_{3-y}Ti_4O_{12}$). Such Cu-deficiency has been suggested previously in the literature to be involved with the high conductivity in the bulk as mentioned above.[24] In this context, it would be plausible that the tendency for Cu-segregation from CCTO grains originates from the volatility of Cu, which thus constitutes the ultimate driving force for the formation and development of the IBLC structure especially for ceramics sintered within $\approx$100 °C of the decomposition temperature.

There is an alternative and plausible explanation for the segregation of this Cu-rich phase though. It may always be prevalent but can only accumulate at the pellet surfaces at sufficiently high T_S due to increased diffusion-related migration associated with the higher sintering temperature. This explanation appears less likely, however, as there were no signs of a Cu-rich phase in the SEM backscattered images on the unpolished and polished surfaces of pellets sintered at or below $T_S = 1025$ °C. Preliminary transmission electron microscopy (TEM) experiments did not yield any conclusive evidence for the presence of such a prevalent Cu-rich phase.

Fig. 6 shows the results from high resolution, quantitative EDAX spot analysis of single CCTO grains, corrected to standard compounds. The Cu contents in terms of the atomic fractions for an average of 25 grains and for the large area average (both for unpolished samples) are displayed vs T_S. The solid horizontal (green) line represents the expected 0.375 Cu cationic ratio (atomic fraction). Cu segregation is clearly evident due to Cu-excess on the unpolished surface above $T_S \geq 1050$ °C. Averaging the Cu content in 25 single grains gave a weak trend towards Cu-loss from within the grain interiors but the trend is statistically just on the limit of significance due to the large experimental error (see error bars). It should be noted though that the data points for single grains in Fig. 6 represent the highest probability of the actual Cu content of the CCTO grains, and it does not seem plausible that the clear trend observed on 6 data points is a statistical coincidence. Large area scans taken from polished surfaces showed no Cu accumulation. Obviously, the Cu-rich phase accumulates at the pellet surfaces during sintering and can be removed by polishing. The error bars represent the first standard deviation of the Cu concentration in the 25 grains investigated. Although the statistical significance of the Cu-loss detected here ($CaCu_{3-y}Ti_4O_{12}$) may be critical, such Cu-loss would be consistent with the increase in bulk conductivity as mentioned before. A high mobility of a secondary Cu-containing phase and accumulation on the pellet surfaces can be unambiguously confirmed.

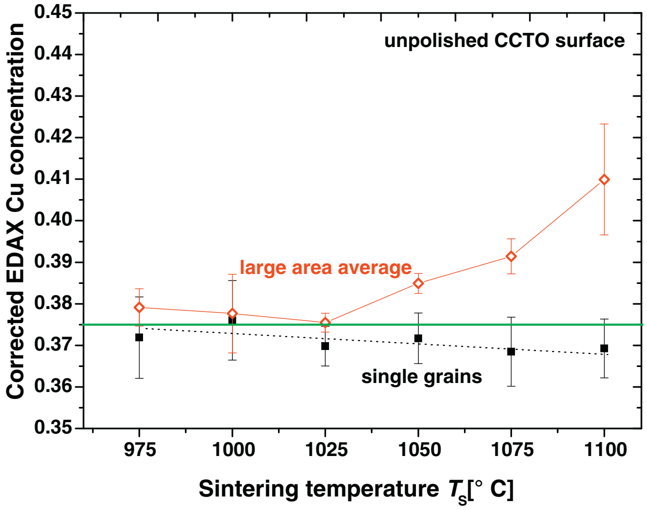

Fig. 6. Quantitative EDAX results corrected to Ca, Cu and Ti standards. Data were obtained from an average of 25 single grains in each pellet (unpolished) (■) and from large area average scans (5 large scans of 150 µm × 150 µm for each sample) of the same pellets (◇). Cu segregation is clearly indicated by the large area scans (red solid line), whereas single grain analysis yielded some indications for Cu-loss from the main $CaCu_{3-y}Ti_4O_{12}$ phase (black dotted line). The bold green solid line indicates the expected 0.375 Cu content based on a stoichiometric cation composition of 1:3:4 for Ca:Cu:Ti. (For interpretation of the references to color in this figure legend, the reader is referred to the web version of the article.)

It should be noted that all changes in dielectric properties with T_S described in the previous section were investigated by IS on well polished pellets. Therefore, the detected dielectric changes cannot be a reflection of the secondary Cu-containing phase.

In the Supporting online materials, Part III, SEM images of all pellets are presented and demonstrate a moderate increase of the mean grain size from 3.0 to 4.8 µm with increasing

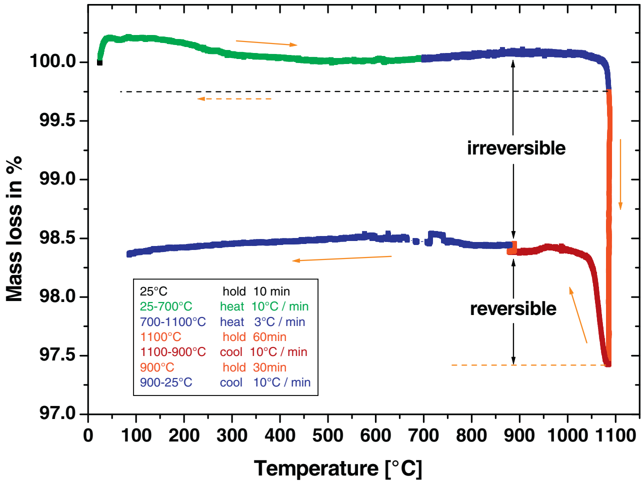

Fig. 7. TG data of CCTO powder. The heating/cooling ramp conditions are indicated in the figure panel. Orange arrows indicate the heating and cooling cycle. The dashed arrow and the dashed line indicate the cooling curve from a second measurement carried out using the same heating conditions but with the cooling cycle starting immediately after reaching 1100 °C (data is not shown explicitly). In the main experiment, irreversible and reversible mass losses were detected. Irreversible mass loss suggests Cu volatilization and/or incomplete re-oxygenation upon cooling, whereas reversible mass loss suggests reduction and complete re-oxidation.

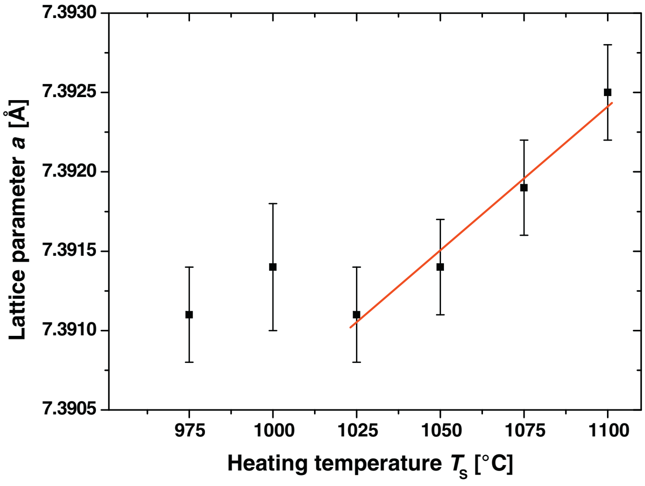

Fig. 8. CCTO lattice parameter ***a*** vs T_S determined from powder XRD using an internal Si standard. For $T_S \geq 1025$ °C an approximately linear increase of ***a*** with increasing T_S is observed (the solid line serves as a guide to the eyes).

$T_S = 1000$–1100 °C. As mentioned above, this increase is insufficient to explain the large increase of GB permittivity ε_2 (Fig. 2).

The grain size distributions are displayed in the Supporting online materials as well.

3.3. *Thermal gravimetry*

Thermal gravimetry (TG) results of CCTO powder are shown in Fig. 7, where the different heat ramps are indicated by different colours. A total mass loss of ≈2.5% was observed after the heating cycle reached 1100 °C and the temperature was held for 60 min at 1100 °C.

A mass gain of ≈1% is observed during the cooling cycle between 1100 and 1000 °C. Therefore, the temperature was held at 900 °C for 30 min to ensure no further significant mass gain occurred. The reversible mass loss/gain may well be attributed to reversible changes in the oxygen content. It is not clear whether this effect is associated with the CCTO phase or the segregated Cu containing phase, e.g.: $CuO \rightarrow Cu_2O \rightarrow CuO$. The irreversible mass loss of ≈1.5% may be due to Cu volatilization and/or incomplete re-oxidation on cooling. A large incomplete re-oxidation of CCTO is less likely, because this would lead to significant changes in the cationic oxidation states, which would be reflected in perceptible changes of the lattice parameter ***a***. Such changes in ***a*** were found to be subtle though as is shown in the next section, and Cu loss due to volatilization is much more likely.

Reduction and reoxidation processes may occur on relatively long time scales because no sign of reversible mass loss (reduction and reoxidation) was found by performing the equivalent experiment on samples cooled immediately from 1100 °C. Such data with the heating ramp set to start the cooling cycle immediately after reaching 1100 °C is not shown explicitly in Fig. 7, but the respective cooling curve is indicated by the dashed arrow and the dashed line at ≈99.75% on the *y*-axis. The heating curves of the two TG experiments coincided as expected. The small irreversible mass loss detected in the second TG experiment may also be attributed to Cu-loss.

3.4. *Lattice parameter determination by XRD*

XRD patterns of powders heated at 975–1100 °C for 12 h were all single-phase (phase pure CCTO), whereas decomposition of the CCTO phase was indicated at 1125 °C. Fig. 8 shows an approximately linear increase of the CCTO lattice parameter ***a*** with increasing T_S for $T_S \geq 1025$ °C (see solid trend line). For $T_S \leq 1000$ °C, no clear trend is obvious. In the literature, an increase of lattice parameter is often associated with a partial reduction of cations and the concomitant increase in cationic radius. The increase in ***a*** detected here is rather small though (maximum change is ≈0.02%) and any potential incomplete re-oxidation after high temperature reduction of the Cu and/or Ti cations in CCTO would be exceptionally small.

3.5. *X-ray absorption near edge spectroscopy (XANES) in CCTO for Cu and Ti K-edges*

Cu K-edge and Ti K-edge absorption spectra for CCTO powders heated at 975 and 1100 °C and overlaid with standard spectra are shown in Figs. 9 and 10, respectively. Inspection of the standard spectra in Fig. 9 shows a shift in the Cu absorption edge position towards higher energy with increasing oxidation state, reflecting the increased binding energy of the 1s core shell with increasing effective nuclear charge. The position of the absorption edge (typically extracted from the position of the edge crest or the first inflection point) has been used to estimate oxidation states but extraction of reliable information can be complicated by differences in edge features for different compounds despite the same nominal redox state.[33] These

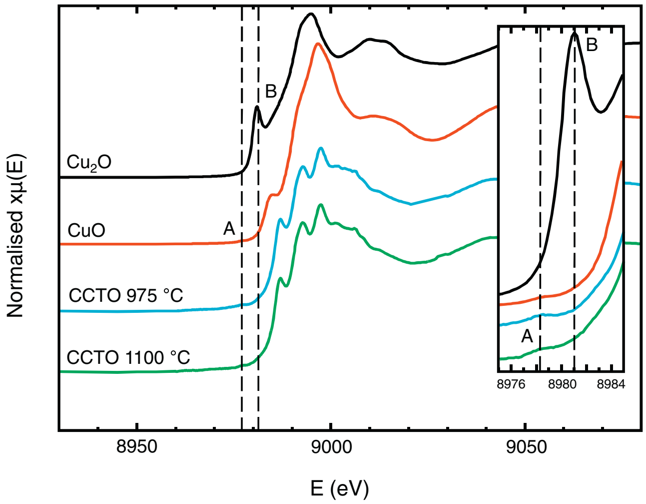

Fig. 9. XANES of the Cu-edge in CCTO powder heated to different temperatures. The figure inset shows the pre-edge region in more detail. There is no indication of Cu^+ in either the 975 or the 1100 °C powder samples.

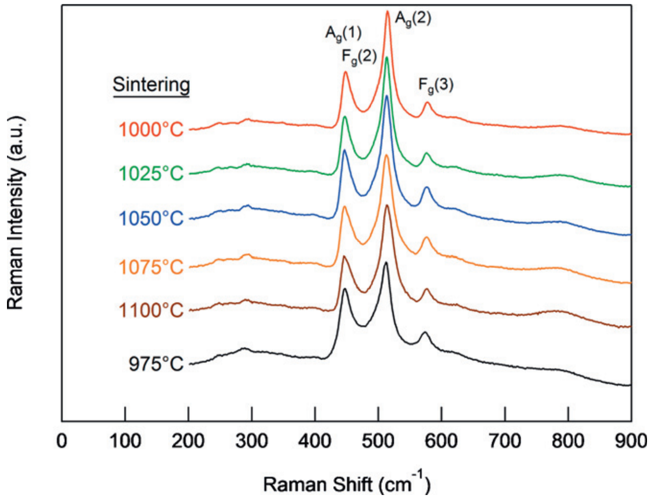

Fig. 11. Raman spectra of CCTO pellets sintered at different temperatures T_S. No sign of phonon mode changes for $T_S = 975–1100$ °C are observed.

differences are related to constructive and destructive interference arising from single and multiple scattering events between the absorber and neighbouring atoms.[34] In addition to the edge position, pre-edge features in XANES spectra can be a powerful tool in determining redox state changes in transition metal compounds (Fig. 9 Inset).[33,35]

The intense feature at ≈8981 eV in the Cu_2O reference spectrum (indicated by the hatched line labeled B) is related to the dipole allowed 1s to 4p transition and is a signature of Cu^+ ions.[36] Similarly for the CuO standard the weak feature at ≈8978 eV (indicated by the hatched line labelled A) is related to the formally dipole forbidden 1s to 3d transition and is characteristic of Cu^{2+} ions.[37] Shimizu et al. showed that the normalized height of this Cu^{2+} peak decreases and the absolute position shifts to higher energy with increasing co-ordination number of the Cu atom.[38] The presence or absence of these features is therefore a useful tool in discriminating between Cu^+ and Cu^{2+} cations. As can be seen from Fig. 9 Inset, the presence of the weak pre-edge feature at ≈8978 eV indicates that the dominant redox state for copper is Cu^{2+} in both CCTO samples, sintered at 975 °C and 1100 °C. No significant difference between the two spectra can be observed suggesting that a potential change in redox state due to T_S must be below the detection limit of this experimental technique. These results compare well with previous data reported by Romero et al.,[15] demonstrating a negligible effect of sintering time (2 and 32 h) on the oxidation state(s) of Cu in CCTO. Fig. 10 shows Ti K-edge absorption spectra for the CCTO powders heated at 975 °C and 1100 °C overlaid with standard spectra from Ti-metal (Ti^0), TiO (Ti^{2+}), Ti_2O_3 (Ti^{3+}) and TiO_2 (Ti^{4+}). TiO_2 exhibits pre-edge features at ≈4972 eV characteristic of Ti^{4+} ions which are replicated in the spectra of both CCTO samples (see figure inset). This indicates that the dominant state for titanium in both samples is Ti^{4+} and within the resolution of the experiment the heat treatment temperatures T_S appears to have no influence on the oxidation state(s) of the Ti ions in CCTO. Generally, it can be concluded that both the Cu and Ti edges in CCTO as determined by XANES are insensitive to changes in the ceramic sintering temperature despite large changes displayed in the electric properties.

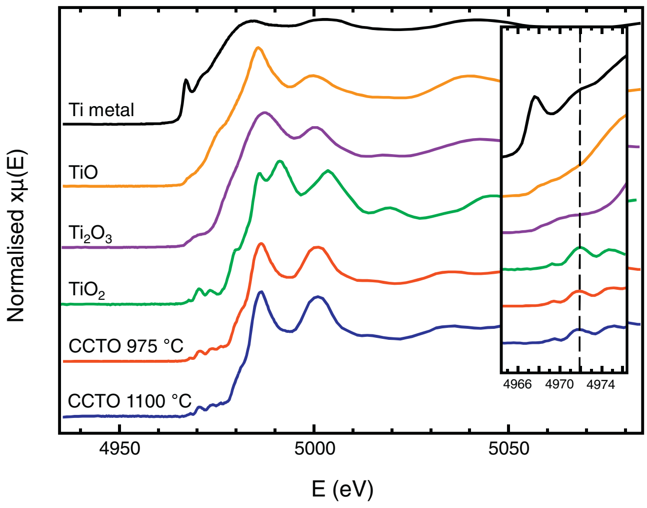

Fig. 10. XANES of the Ti-edge in CCTO powder heated to different temperatures. The figure inset shows the pre-edge region in more detail. The pre-edge feature indicates the presence of octahedrally coordinated Ti^{4+} in both the 975 °C and the 1100 °C powder samples. There is no indication of any reduced Ti-species.

3.6. Raman spectroscopy

Raman spectra of CCTO pellets sintered at different T_S are depicted in Fig. 11. The detected Raman modes are in agreement with previous reports,[39–41] where the mode with a Raman shift of 445 cm^{-1} was identified as $A_g(1)$ which forms a double peak structure with the $F_g(2)$ mode at a slightly higher Raman shift. The modes at 511 and 576 cm^{-1} were identified as $A_g(2)$ and $F_g(3)$, respectively. The $A_g(1)$, $A_g(2)$ and $F_g(2)$ modes arise from TiO_6 rotation-like lattice vibrations, whereas the $F_g(3)$ mode is associated with a O–Ti–O anti-stretching vibration.[39] No changes in the phonon mode structure are evident from the

Raman Spectroscopy data. Although significant changes in electric properties have been detected for pellets sintered at different T_S no changes are obvious in the Ti-related lattice vibrations. This is in agreement with Ref.[15] where no significant changes in the Raman spectra were found for CCTO sintered at 1100 °C with different sintering times of 2 and 32 h. It can be concluded that Raman Spectroscopy is insensitive to changes in sintering time and/or sintering temperature of CCTO ceramics.

4. Conclusions

By changing the sintering temperature of CCTO ceramics from 975 to 1100 °C massive variations in the electric properties were detected. The bulk and GB permittivity increased by factors of ≈2 and 300, respectively, whereas the bulk resistivity decreased by a factor of $\approx 10^3$. Despite such dramatic changes in electric properties, it is difficult to detect significant changes in the compound chemistry and especially changes in the oxidation state(s) of the Cu and Ti ions which are presumably linked to the bulk conductivity. Such chemical changes must exist though and it is concluded that the CCTO electric properties must be highly sensitive to exceptionally small chemical changes. Any valence and subtle structural changes induced by T_S were found to be below the resolution limit of XANES at the Cu and Ti K-edges and Raman spectroscopy. Quantitative EDAX analysis indicated a weak trend for Cu-loss within individual CCTO grains with increasing T_S. Segregation of a Cu-rich phase out of CCTO ceramics at $T_S \geq 1050$ °C was unambiguously detected. This secondary Cu-rich phase may exhibit high mobility, accumulate at the pellet surfaces and, in part, may volatilize at ≈1100 °C as demonstrated by an irreversible ≈1.5% mass loss detected by thermal gravimetry. Furthermore, the presence of a reversible ≈1% mass gain detected on cooling provides evidence for changes in oxygen stoichiometry due to reduction (on heating) and reoxidation (on cooling) processes in samples heat treated at 1100 °C in air for at least 60 min.

It is concluded that increasing the sintering temperature T_S promotes the formation of the IBLC structure. The dramatic differences in bulk and GB electric properties of CCTO ceramics are primarily driven by subtle chemical changes such as Cu segregation from the bulk to the grain boundary regions, promoted by the heat treatment conditions employed.

Acknowledgments

We thank the European Union (EU) for funding this work under the NUOTO project and under the FP7/2007-2013 grant agreement no 226716. Use of the National Synchrotron Light Source, Brookhaven National Laboratory, was supported by the U.S. Department of Energy, Office of Science, Office of Basic Energy Sciences, under Contract No. DE-AC02-98CH10886. We are grateful for allocation of beamtime at the ELETTRA light source, which was carried out as part of the EPSRC DIAMOND research program under grant EP/F055412/1. We thank B. Ravel and G. Aquilanti for assistance in acquisition of XAS data and A. Feteira for initial TEM measurements. RS acknowledges a Ramón y Cajal fellowship from the Ministerio de Ciencia e Innovación in Spain. NCH is grateful to the Royal Academy of Engineering and Nuclear Decommissioning Authority for funding. ML and DCS are grateful to the EPSRC for funding, EP/G005001/1.

Appendix A. Supplementary data

Supplementary data associated with this article can be found, in the online version, at doi:10.1016/j.jeurceramsoc.2012.03.040.

References

1. Ramirez AP, Subramanian MA, Gardel M, Blumberg G, Li D, Vogt T, Shapiro SM. *Solid State Commun* 2000;**115**:217.
2. Homes CC, Vogt T, Shapiro SM, Wakimoto S, Ramirez AP. *Science* 2001;**293**:673.
3. Chung S-Y, Kim I-D, Kang S-JL. *Nat Mater* 2004;**3**:774.
4. Sinclair DC, Adams TB, Morrison FD, West AR. *Appl Phys Lett* 2002;**80**:2153.
5. Schmidt R, Sinclair DC. *Chem Mater* 2010;**22**:6.
6. Zhu Y, Zheng JC, Wu L, Frenkel AI, Hanson J, Northrup P, Ku W. *Phys Rev Lett* 2007;**99**:037602.
7. Sebald J, Krohns S, Lunkenheimer P, Ebbinghaus SG, Riegg S, Reller A, Loidl A. *Solid State Commun* 2010;**150**:857.
8. Fang T-T, Liu JP. *Chem Mater* 2005;**17**:5167.
9. Liu JP, Sui Y, Duan C-G, Mei W-N, Smith RW, Hardy JR. *Chem Mater* 2006;**18**:3878.
10. Adams TB, Sinclair DC, West AR. *Adv Mater* 2002;**14**:1321.
11. Liu J, Smith RW, Mei W-N. *Chem Mater* 2007;**19**:6020.
12. West AR, Adams TB, Morrison FD, Sinclair DC. *J Eur Ceram Soc* 2004;**24**:1439.
13. Ferrarelli MC, Adams TB, Feteira A, Sinclair DC, West AR. *Appl Phys Lett* 2006;**89**:212904.
14. Li M, Feteira A, Sinclair DC, West AR. *Appl Phys Lett* 2006;**88**:232903.
15. Romero JJ, Leret P, Rubio-Marcos F, Quesada A, Fernández JF. *J Eur Ceram Soc* 2010;**30**:737.
16. Li M, Sinclair DC, West AR. *J Appl Phys* 2011;**109**:084106.
17. Ferrarelli MC, Sinclair DC, West AR, Dabkowska HA, Dabkowski A, Luke GM. *J Mater Chem* 2009;**19**:5916.
18. Lunkenheimer P, Fichtl R, Ebbinghaus SG, Loidl A. *Phys Rev B* 2004;**70**:172102.
19. Krohns S, Lunkenheimer P, Ebbinghaus SG, Loidl A. *Appl Phys Lett* 2007;**91**:022910.
20. Adams TB, Sinclair DC, West AR. *Phys Rev B* 2006;**73**:094124.
21. Capsoni D, Bini M, Massarotti V, Chiodelli G, Mozzatic MC, Azzoni CB. *J Solid State Chem* 2004;**177**:4494.
22. Deng G, Xanthopoulos N, Muralt P. *Appl Phys Lett* 2008;**92**:172909.
23. Adams TB, Sinclair DC, West AR. *J Am Ceram Soc* 2006;**89**:3129.
24. Li J, Sleight AW, Subramanian MA. *Solid State Commun* 2005;**135**:260.
25. Li J, Subramanian MA, Rosenfeld HD, Jones CY, Toby BH, Sleight AW. *Chem Mater* 2004;**16**:5223.
26. Barsukov E, Macdonald J. *Impedance Spectroscopy: Theory, Experiment and Applications*. Hoboken: John Wiley & Sons Inc; 2005.
27. Schmidt R. Impedance spectroscopy of electroceramics. In: Lin PB, editor. *Ceramic Materials Research Trends*. Hauppauge: Novascience Publishers; 2007. p. 321.
28. Ravel B, Newville M. *J Synchr Rad* 2005;**12**:537.
29. Irvine JTS, Sinclair DC, West AR. *Adv Mater* 1990;**2**:132.
30. Bender BA, Pan MJ. *Mater Sci Eng B* 2005;**117**:339.
31. Shri Prakash B, Varma KBR. *Physica B: Cond Mat* 2006;**382**:312.
32. Ferrarelli MC, Nuzhnyy D, Sinclair DC, Kamba S. *Phys Rev B* 2010;**81**:224112.
33. Farges F, Brown GE, Rehr JJ. *Geochim Cosmochim Acta* 1996;**60**:3023.

34. Farges F, Etcheverry M-P, Scheidegger AM, Grolimund D. *Appl Geochem* 2006;**21**:1715.
35. Chalmin E, Farges F, Brown GE. *Contrib Mineral Petrol* 2009;**157**:111.
36. Maurizio C, d'Acapito F, Benfatto M, Mobilio S, Cattaruzza E, Gonella F. *Eur Phys J B* 2000;**14**:211.
37. Arletti R, Dalconi MC, Quartieri S, Triscari M, Vezzalini G. *Appl Phys A* 2006;**83**:239.
38. Shimizu K, Maeshima H, Yoshida H, Satsuma A, Hattori T. *Phys Chem Chem Phys* 2001;**3**:862.
39. Kolev N, Bontchev RP, Jacobson AJ, Popov VN, Hadjiev VG, Litvinchuk AP, Iliev MN. *Phys Rev B* 2002;**66**:132102.
40. Valim D, Souza Filho AG, Freire PTC, Fagan SB, Ayala AP, Mendes Filho J, Almeida AFL, Fechine PBA, Sombra ASB, Staun Olsen J, Gerward L. *Phys Rev B* 2004;**70**:132103.
41. Almeida AFL, Fechine PBA, Graca MPF, Valente MA, Sombra ASB. *J Mater Sci: Mater Electron* 2009;**20**:163.